Asociación Argentina
de Mecánica Computacional

Mecánica Computacional Vol XXIX, págs. 8837-8858 (artículo completo)
Eduardo Dvorkin, Marcela Goldschmit, Mario Storti (Eds.)
Buenos Aires, Argentina, 15-18 Noviembre 2010

NUMERICAL STUDY ON WELLBORE STABILITY ANALYSIS CONSINDERING VOLUMETRIC FAILURE

Michel N. Zahn[a], Lúcia Carvalho Coelho[a], Luiz Landau[a] and José Luis Drummond Alves[a]

[a]*Laboratório de Métodos Computacionais em Engenharia, Universidade Federal do Rio de Janeiro, Caixa Postal 68.552, CEP 21941-972, lamce@lamce.coppe.ufrj.br*

Keywords: Wellbore stability, Plasticity, Cap Models.

Abstract. When a wellbore is drilled, the equilibrium in-situ stress is changed. In order to support the stress relief induced by the drilling and to prevent hydrocarbon influx into the cavity, the borehole is filled with a fluid. These operations create new stresses configurations. A main point in wellbore projects is the definition of the drilling fluid density to keep the wellbore stable. The upper bound to the fluid density is the collapse stress that is the limit to shearing. The lower bound is the fracture stress that limits the tensile failure. The fluid densities between these limits is named safe mud weight window. Conventional wellbore stability analysis usually considers the effects of shear or tensile failure. Recent physical models pointed the possibility of compactive volumetric failure around boreholes. Other numerical studies showed that this type of failure may be attained by stress level compatible with reservoirs in under production in high porosity rocks. This paper applies numerical modeling by finite element method with ANSYS® software to study stability of oil wells. It simulates the compactive behavior of rocks using a cap plasticity model. The cap model data was collected from literature. Parametric studies were conducted in horizontal wellbores to evaluate the conditions of volumetric failure to occur. The study pointed the tangential stress concentration as a critical condition for volumetric failure around boreholes.

1 INTRODUCTION

Hydrocarbon exploitation in marine coast of Brazil requires new technologies for its economic feasibility. Pre-Salt reserves are located in Santos Basin at 290 km from the coast. The water depth is about 1900 to 2400 meters and the reservoirs are located at 5000 meters underground, below a salt layer that may reach 2000 meters. The exploitation of these reserves require unconventional well technologies to make it feasible from an economic point of view.

The use of directional and horizontal wells has been increased in the last years, following the advances in the techniques on drilling and completing these wells. Horizontal wells present advantages in relation to vertical wells, as it has a bigger area exposed to flow. In offshore environments it is an additional advantage, since locating the platform is critical due to sea conditions.

These unconventional environments and well geometries led to the problem of wellbore stability analysis and sand prediction. This kind of problem has a big impact on wellbore costs.

Prediction models for wellbore stability analysis are based on rock mechanics models. The first model based on rock mechanics for this kind of problem was proposed by Bradley (1979). Several models based on continuous mechanics were developed since then. The assumptions of these models vary from simple elastic models to more elaborated elastic-plastic models. Morita (2004) proposed an analytical procedure based on elasticity to evaluate the stress state around the borehole. The stress level is compared to a compression or tensile failure criteria to evaluate stability. The most used failure criteria are Drucker-Prager, Mohr-Coulomb, modified Lade criterion (Ewy, 1999) or Hoek and Brown (Zhang and Zhu, 2007). Tensile criterion usually consists in the comparison of the minimum effective stress to the tensile strength of the rock.

These models are considered very conservative, since attaining the limit stress in a point around the borehole does not imply in instability. Numerical methods based on plasticity theory, such as finite difference or finite elements methods, present the advantage of showing the extent of the damaged region, leading to a better indicator of instability. These models usually consider two kinds of failure around the wellbore: shear failure and tensile failure. They became more complex, as they incorporated other physics associated to instability: poroelastic models (Detournay and Cheng, 1993), thermoporoelastic (Wang and Desseault, 2003), chemo-thermoporoelastic (Yu et al, 2001) and its versions associated to plasticity theory. Advances in elastic-plastic models to improve stability indicators were developed, such as bifurcation theory and localization of deformation along shear bands. The rock microstructure has been incorporated through the Cosserat continuum model (Papanastasiou and Vardoulakis, 1988, 1989) or gradient elastoplasticity (Zervos et al., 2001), which uses terms of strain gradient as state variable.

The models described above depend on a realistic constitutive model that must be able to reproduce the several failure modes around boreholes. Experimental studies show that rocks under high confining pressures can reach the hydrostatic stress strength. Once this limit is attained, severe compaction of porous media occur, leading to porosity and permeability reduction. This work names this kind of failure as volumetric failure.

Coelho et al. (2005) presented a numerical study on a wellbore drilled in a reservoir from Brazilian coast and showed that volumetric failure can be reached under those reservoir conditions. These results are compatible with experimental studies. Haimson (2007) identified a breakout pattern for porous rocks, distinct of those identified for rocks of lower porosity. Porous rocks presented a slit mode failure, surrounded by a highly compacted material,

suggesting an "empty" compaction band.

This work presents a study on the conditions for volumetric failure occurrence around boreholes. It uses a constitutive model that is able to predict shear failure, tensile failure and compaction failure around boreholes. The data used in these analyses were taken from literature on porous rocks. Parameters that impact on wellbore stability were evaluated.

The numerical modeling of wellbore stability analysis is made considering small strain and small displacement finite element method and classical associated plasticity theory. The software used was ANSYS® and the mesh is based on linear triangles.

The well configuration studied was a horizontal wellbore under plane strain conditions. To take advantage of the problem symmetry, the mesh consisted of ¼ of the geometry. The rock is treated as an isotropic and homogeneous continuum medium. The constitutive model used was the cap model as implemented by ANSYS®.

2 FAILURE MODES AROUND BOREHOLES

Wellbore stability during drilling consists on evaluating the drilling fluid weight to mantain the borehole wall integrity. It means that pressure on the boreface must be less than formation fracture pressure and more than the collapse pressure to avoid fluid losses or borehole breakouts. These phenomena are associated to tensile failure (figure 1a) or shear failure (figure 1b), respectively.

Haimson and Song (1998) described two distinct breakout patterns in Berea sandstone under drilling in true triaxial laboratory conditions. For lower porosity (17%), the breakout showed dog-ear geometry (figure 1b). For a higher porosity (22.5%), slit-mode breakout (figure 1c) was obtained during the drilling. Haimson and Lee (2004) observed that these distinct modes of failure are dependent not only on porosity, but also on sandstone composition. Haimson´s work associated these fracture-like breakouts with empty compaction bands. This failure mode is not clear under field conditions.

Triaxial tests on rocks under higher confining pressures are described by Baud et al. (2004, 2006). They describe the volumetric behavior of rocks based in the stress-strain curve as shown in figure 2 for Tavel limestone. In this figure, compression is positive. At lower confining stress, the volumetric strain is dilative until point C' of mean stress- volumetric strain curve (figure 2b). At a confining stress of 100 MPa, the rock first experiences compaction and then dilates. Under higher confining pressures the rock shows a compaction behavior. These characteristic points are presented in figure 3 in the differential stress-mean stress space for Indiana limestone. It can be seen the contour of a cap that limits the strength to rock hydrostatic compression. This graphic delimits different volumetric strain behavior: at lower confining pressures, dilation occurs. This region is followed by a brittle-ductile transition, and then the compaction cap is attained as confining pressure increases. Undergoing further compression, the cap expands in the stress space, until the material is so compacted that it returns to a dilation behavior. The micromechanisms associated to these failure modes are presented in figure 4. In the dilation regime, rock fails by the formation of a shear band; in the brittle-ductile transition, there is a mixed mode of deformation between dilatation and compaction. The cap delimits distinct mechanisms: at higher deviator stresses, the so-called shear enhanced compaction occurs, by the development of a compaction band. Close to the first stress invariant axis, the dominant deformation mechanism is pore collapse, which corresponds to a more diffuse deformation pattern.

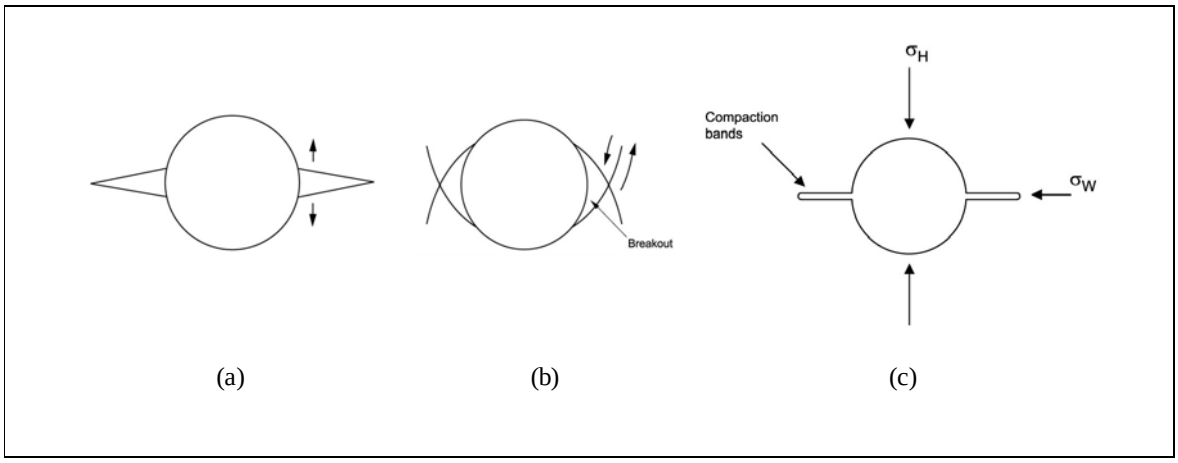

Figure 1: Failure modes around wellbores (a) tensile failure (hydraulic fracturing); (b) dog-ear shape breakout; (c) fracture-like breakout.

The most common elastic-plastic constitutive models used in wellbore stability analysis are shear failure models such as Drucker-Prager and Mohr-Coulomb, associated to some tensile failure criteria. These models are representative of lower porosity rock behavior. The compaction mechanisms can be predicted by cap models (Fjaer et al., 2008).

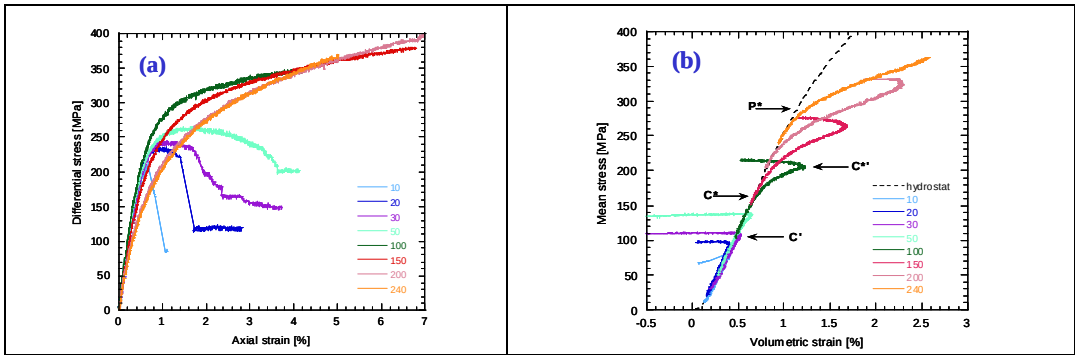

Figure 2: Triaxial tests for Tavel limestone (a) differential stress-axial strain; (b) Mean stress-volumetric strain (from Vajdova et al, 2004)

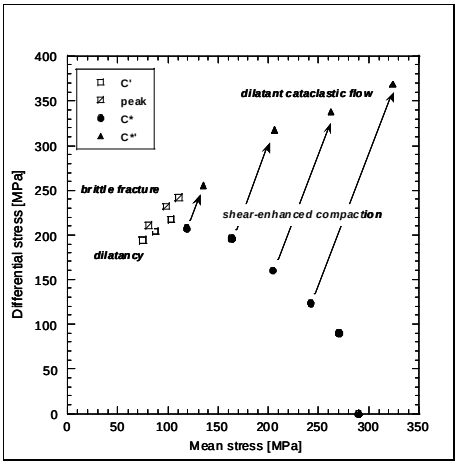

Figure 3: Triaxial tests for Indiana limestone (a) differential stress-axial strain; (b) Mean stress-volumetric strain (from Vajdova et al, 2004)

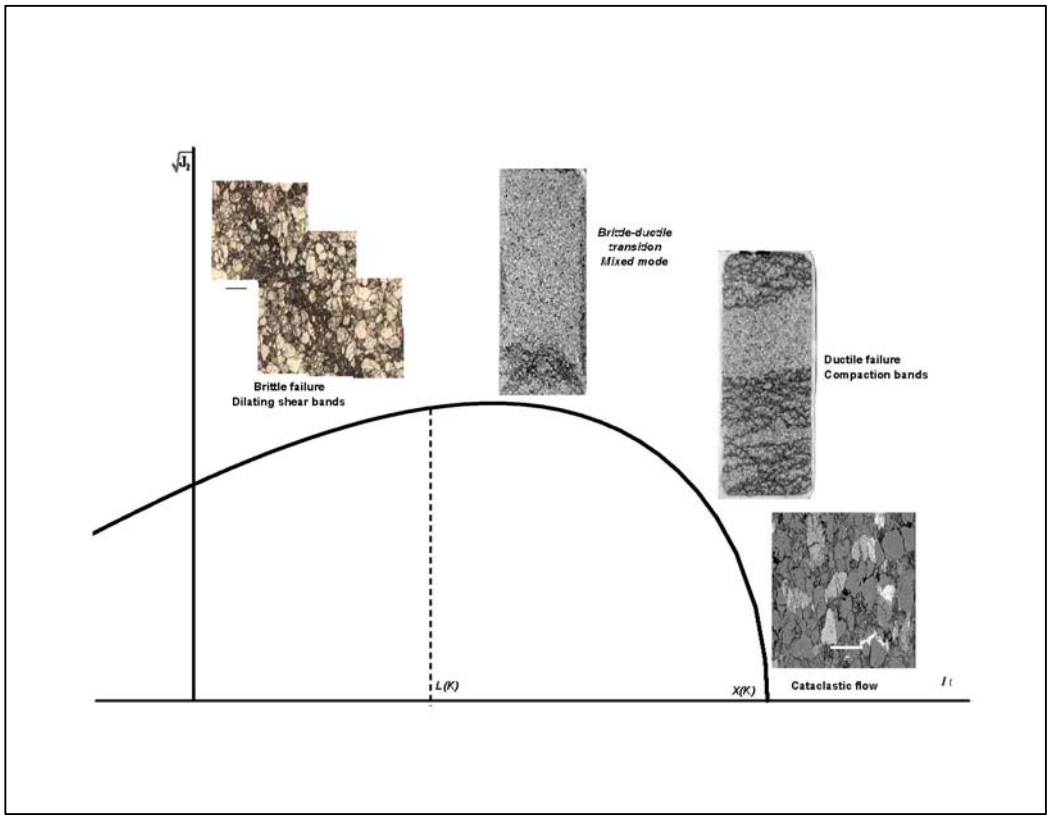

Figure 4: Micromechanisms associated to distinct failure modes
(from: Baud et al, 2008)

3 STRESS STATE AROUND BOREHOLES

An underground rock mass is in equilibrium condition under compressive in-situ stress state, which can be decomposed in relation to a Cartesian coordinates system as vertical stress, parallel to the depth direction and two horizontal stresses: a major horizontal stress (S_H) and a minor horizontal stress (S_h). Changes in this stresses are introduced by the drilling and production operations.

The governing poroelastic equations for a homogeneous isotropic media, considering the absence of body forces and fluid sources, are given by (Wang, 2000):

$$\Delta\sigma_{ij} = \lambda\varepsilon_{kk}\delta_{ij} + 2G\varepsilon_{ij} - \alpha\Delta p\delta_{ij} \tag{1}$$

$$\Delta p = M\left(\varsigma - \alpha\varepsilon_{kk}\right) \tag{2}$$

$$\sigma_{ij,j} = 0 \tag{3}$$

$$\frac{d\varsigma}{dt} + q_{i,i} = 0 \tag{4}$$

$$q_i = -\kappa p_{,i} \tag{5}$$

Where tensile stresses are positive, $\Delta\sigma_{ij}$ is the total stress change tensor, ε_{ij}, the solid strain tensor, Δp is the pore pressure differential, ς is the variation of fluid content, ε_{kk} is the volumetric strain, λ and G are the Lamé´s parameter for the porous rock, α is the Biot's effective stress coefficient, M, the Biot modulus and δ_{ij} is Kronecker delta.

The parameters that govern balance laws are:

$$\kappa = \frac{k}{\mu} \tag{6}$$

κ is the mobility coefficient, k is the permeability coefficient and μ is the fluid viscosity.

Applying the constitutive relations to the equilibrium condition and expressing the deformation term as displacement derivative, the governing equation in terms of displacements is given by:

$$\left(\frac{G}{1-2\nu}\right)\left(\frac{\partial^2 u_k}{\partial x_i \partial x_k} + \frac{\partial^2 v}{\partial z \partial y} + \frac{\partial^2 w}{\partial z^2}\right) + G\nabla^2 u_i = \alpha \frac{\partial p}{\partial x_i} - F_i \tag{7}$$

Under steady state conditions, the the equation governing the pore pressure field uncouples (Detournay and Cheng, 1993):

$$\Delta p = -M\alpha\varepsilon \tag{8}$$

As the well is drilled and material is removed, a stress relief occurs. If the cavity is not fulfilled with fluid, the equilibrium is attained by tangential stress concentration. The drilling fluid introduces a radial pressure against the borehole wall. This pressure acts as a support to the boreface and relieves the generated tangential stress.

The stress state around the borehole may vary according to its radius and inclination angle. This variation depends on many factors as the wellbore direction related to in-situ stresses, the in-situ stresses magnitude, the rheology of the rocks and wellbore geometry.

As one moves from the borehole into the formation, the stresses tend to reach the in-situ stresses. According to Rocha and Azevedo (2009), the usual stress configuration around the well is: tangential stress is the major principal stress; axial stress is the intermediate stress although in lower depths it may become the major stress and radial stress is the minor principal stress.

4 ELASTIC PLASTIC MODEL

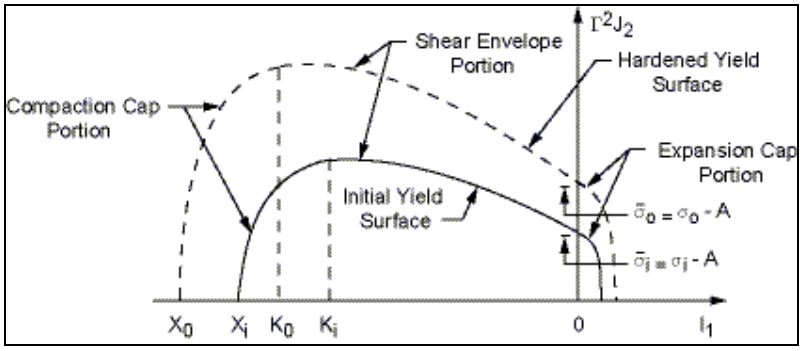

Figure 5: Cap model plasticity yield surface; tensile stress is positive (from Release 11.0 Documentation for ANSYS)

The analyses were made using ANSYS® cap model (figure 5). The formulation of this model is described in Theory Reference for Ansys and Ansys Workbench from Ansys documentation and is briefly summarized here.

It consists on a shear failure surface associated to an elliptical cap for compressive volumetric failure and a tensile cap, described by the following equation:

$$\begin{aligned} &Y(\sigma, K_0, \sigma_0) = Y(I_1, J_2, J_3, K_0, \sigma_0) \\ &= \Gamma^2(\beta, \Psi) J_2 - Y_c(I_1, K_0, \sigma_0) Y_t(I_1, \sigma_0) Y_s^2(I_1, \sigma_0) \end{aligned} \tag{9}$$

where :

Γ : Lode's angle function,

Y_c : compressive cap function

Y_t : tensile cap function

Y_s : shear failure surface

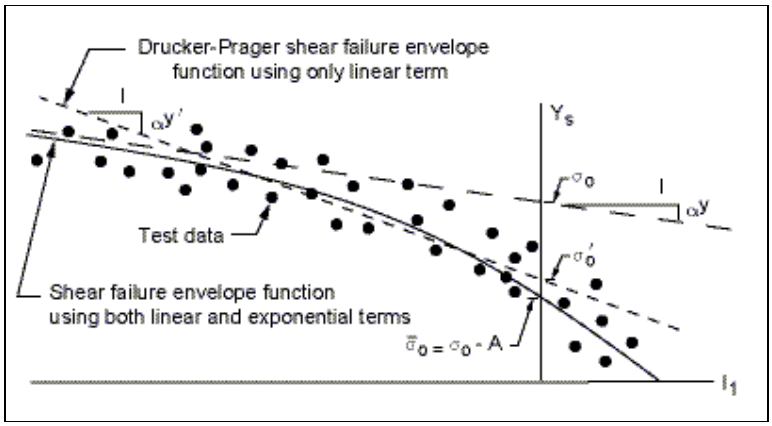

Figure 6: Shear yield function (from Release 11.0 Documentation for ANSYS)

The shear failure surface (figure 6) is described by:

$$Y_S(I_1, \sigma_0) = \sigma_0 - Ae^{(\beta I_1)} - \alpha I_1 \tag{10}$$

$$Y_c(I_1, K_0, \sigma_0) = 1 - H(K_0 - I_1)\left(\frac{I_1 - K_0}{R_c Y_s(K_0, \sigma_0)}\right)^2 \tag{11}$$

$$Y_t(I_1, \sigma_0) = 1 - H(I_1)\left(\frac{I_1}{R_t Y_s(0, \sigma_0)}\right)^2 \tag{12}$$

In the above expressions, I_1 is the first stress invariant, σ_o is a constant associated to cohesion, A, β and α are constants obtained from experiments, R_c and R_t is the ratio between the main axis in I_1 direction and main axis in J_2 direction of the compressive cap and tensile cap, respectively. The parameter K_o is the value of I_1 at intersection point between the shear failure surface and the elliptical cap. Function H is the Heaviside function,

which assumes the values:

$$H = \begin{cases} 0, \text{ para } I_1 < K_o \\ 1, \text{ para } I_1 > K_o \end{cases} \tag{13}$$

The parameters K_0 and X_0 are associated by:

$$K_0 = X_0 + R_c Y_s(K_0, \sigma_0) \tag{14}$$

The function Y_c is an elliptical function associated to Heaviside function, as show figure 7(a).

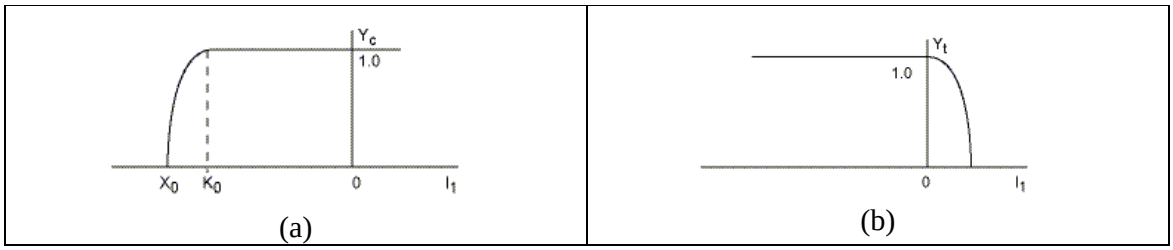

Figure 7: (a) Elliptical compressive cap; (b) Elliptical tensile cap (from Release 11.0 Documentation for ANSYS)

The tensile cap (figure 7(b) is similar to the compressive cap, but it is fixed in the stress space and depends only on the first stress invariant and the cohesive term:

$$Y_t(I_1, \sigma_0) = 1 - H(I_1)\left(\frac{I_1}{R_t^y Y_s(0, \sigma_0)}\right)^2 \tag{15}$$

The influence of the third deviator stress invariant is introduced by the function of Lode's angle β and the triaxial compressive strength:

$$\Gamma(\beta, \Psi) = \frac{1}{2}(1 + sen3\beta + \frac{1}{\Psi}(1 - sen3\beta)) \tag{16}$$

Lode's angle is given by:

$$\beta(J_2, J_3) = -\frac{1}{3} sen^{-1}\left(\frac{3\sqrt{3}J_3}{2J_2^{3/2}}\right) \tag{17}$$

These relations are shown in figure 8:

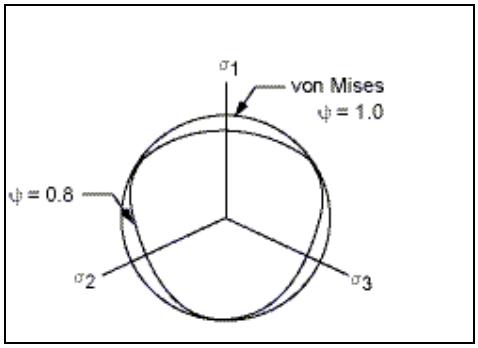

Figure 8: Failure surface in deviatoric plane (from Release 11.0 Documentation for ANSYS)

This work assumes a perfect elastic-plastic shear surface and a isotropic strain hardening compressive cap, defined by:

$$\varepsilon_v^p = W_1^c\{e^{(D_1^c - D_2^c(X_0 - Xi))(X_0 - Xi)} - 1\} \tag{18}$$

The parameter X_i represents actual position of cap parameter X, W_1^c is the maximum allowed plastic strain, D_1^c and D_2^c are experimental adjustment parameters for the hardening function.

5 MODELING PROCEDURE

Two loading steps were considered: the first corresponds to drilling phase and the second to steady state production phase.

Stability during drilling was modeled considering no fluid flow between the wellbore and the rock. The values of far-field effective stresses were applied to the boundaries of the model, as well as a pressure on the cavity, which is equivalent to the differential fluid pressure between the fluid in the cavity and reservoir pressure.

To simulate stability during production, the drawdown pressure was applied on the cavity face and poroelastic effects were taken into account, induced by fluid flow from the reservoir to the wellbore. In this work, it was assumed that one-phase fluid saturates porous media. The model assumes that at the outer boundary the pore pressure remains unaltered. This drainage radius may not be realistic, but it was assumed reasonable for the purpose of evaluating the stresses in the vicinity of the wellbore. It must be taken from a qualitative point of view.

To simulate these effects with ANSYS, the approach was to explore the analogy between poroelasticity and thermoelasticity.

5.1 Thermoelasticity and poroelasticity analogy

Fjaer et al. (2008) showed the analogy between poroelastic stresses, described by equation 1 (rewritten below) and thermoelastic stresses (equation 19):

$$\sigma_{ij} = \lambda_{fr}\varepsilon_{kk}\delta_{ij} + 2G\varepsilon_{ij} + \alpha\Delta p\delta_{ij}$$

$$\sigma_{ij} = \lambda\varepsilon_{kk}\delta_{ij} + 2G\varepsilon_{ij} + 3\alpha_T K\Delta T\delta_{ij} \tag{19}$$

The term that couples the thermal/pore pressure field to the stress analysis is the parameter α_T (thermal stress expansion coefficient) or α (Biot´s effective stress coefficient), respectively. Manipulating this term, poroelastic stress may be obtained by a thermoelastic analysis by making:

$$\alpha_T = \frac{\alpha}{3K} \tag{20}$$

where 1/K is the rock compressibility

5.2 Procedure validation

To check the procedure, the hollow poroelastic cylinder was modeled. The geometric model consists on a cylinder with a 2 meters internal radius and 10 meters external radius, with an internal pressure of 15 MPa. The mesh takes advantage of symmetry and represents ¼ of the geometry. It has 4753 nodes and 4608 linear isoparametric elements. Figure 9 shows de mesh. A poroelastic analysis was done by analogy with thermoelastic analysis. The elastic parameters used were an elastic modulus of 1200 MPa and Poisson ratio of 0.2. The thermal analysis was coupled to the structural analysis through the compressibility of the rock analogous to the thermal expansion coefficient following equation 20. The values adopted for Biot effective stress coefficient was 1 and $\alpha_t = 0.0005$.

Pore pressure field obtained through this analysis is presented in figure 10. It is compared to the analytical solution described by Wang (2000), and is shown in figure 11. It presents a good agreement between both analysis. The differences in the stresses in the vicinities of the wellbore may be attributed to the fact that in finite element analysis they are evaluated at the integration point rather then the nodal point at the boreface.

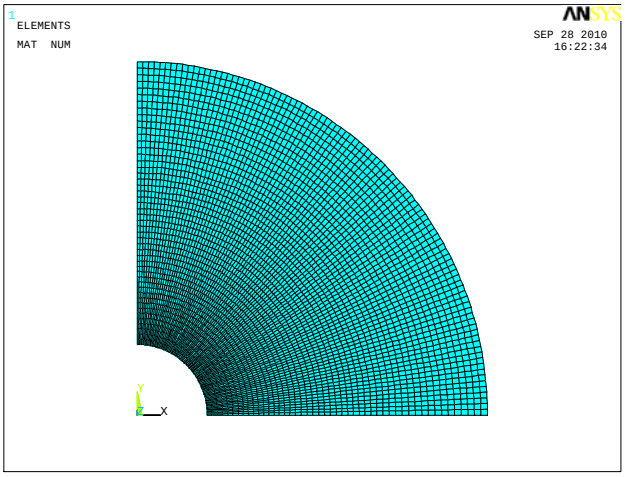

Figure 9: Hollow cylinder mesh

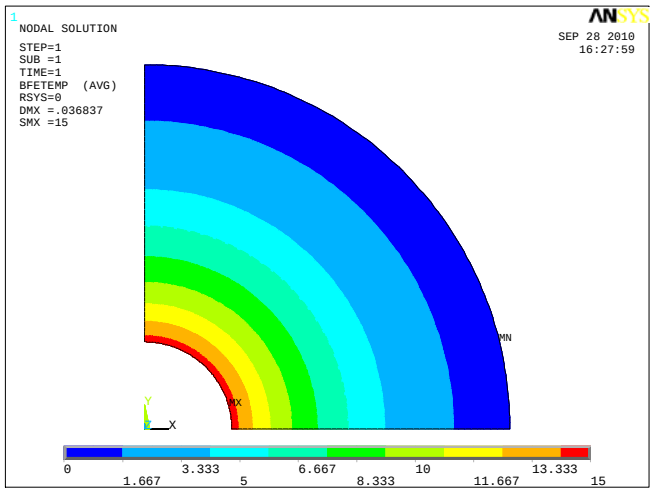

Figure 10:Pore pressure field

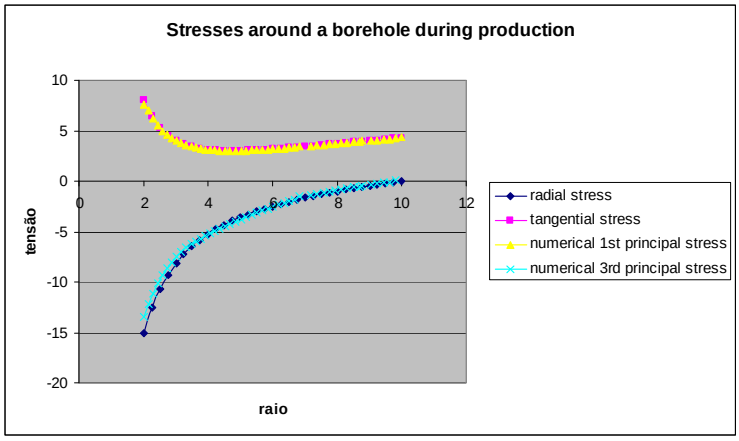

Figure 11: Comparison between analytical and numerical solution for stress states in the poroelastic hollow cylinder (compression is positive)

6 PARAMETRIC STUDY OF A HORIZONTAL WELLBORE

6.1 Basic model

The basic model used for comparison is a open-hole horizontal wellbore, 8.5" diameter, drilled in a carbonate from Campos Basin. The data was obtained from Coelho et al (2006). It is presented in table 1.

Horizontal wellbore geometry takes advantage of the symmetry of the problem. The wellbore is represented by ¼ of the circle and the external boundary is 50 meters from the wellbore axis. The numerical model consists in a mesh with 1671 nodes and 3088 elements (figure 12). The in-situ stress state is represented by the introduction of a distributed vertical loading on the top of external boundary, which value is equivalent to the vertical in-situ stress and a lateral loading on the external boundary which value is the value of in-situ horizontal stress. The in-situ stress in the axial direction is simulated by setting an initial stress state equivalent to its value The pressure on the wellbore wall is represented by a pressure on the bore face.

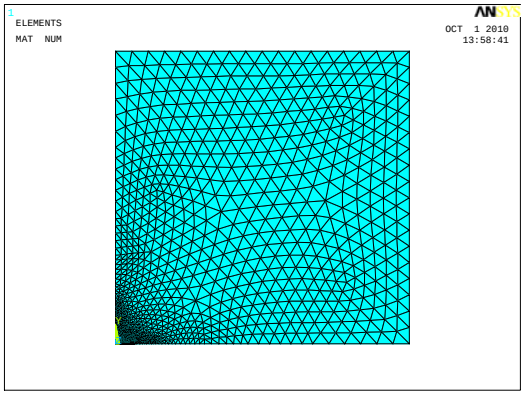

Figure 12: Finite element mesh

It is assumed that the horizontal in-situ stresses are isotropic. Loading condition used in this study assumes two load steps. The first one is the drilling phase, when the far-field in-situ stresses are applied to the boundaries as described above. A pressure at the borehole

equivalent to the difference between the fluid in the formation and the fluid in the cavity is set.

The second load step assumes that the fluid flows into the borehole and poroelastic effects are then simulated with the thermoelastic analogy procedure described in 5.2. The differential pore pressure stress at the boreface is considered by applying a tensile stress at this face equivalent to this differential.

Table 2 presents the reservoir data used in this work.

Parameter	Value
Elastic modulus (MPa)	1200.
Poisson ratio	0.2
σ_o (MPa)	4.92
α	0.589707
Xo (MPa)	-108.
R_c	2.2
R_t	1.0
W	0.05
β	1.0
A	0.0
D_1^c	0.012
D_2^c	0.0

Table 1: Mechanical properties for carbonate rock for Campos basin.

Vertical effective in-situ stress (MPa)	Horizontal effective in-situ stress (MPa)	Static pressure in reservoir (MPa)
32.0	8.0	32

Table 2: Reservoir data.

To understand the effects of volumetric failure around the wellbore, analysis considering only shear failure in the compressive domain and analysis with the cap model were made. An evaluation of the stresses conditions on volumetric failure around the wellbore was done by analyses with parametric changes for different in-situ horizontal stress vs vertical stress ratio and different values of pressure on the borehole wall. Finally, a poroelastic-plastic analysis to simulate production phase under steady-state flow conditions is presented.

6.2 Shear failure analysis

Shear failure analysis was conducted by using the same failure surface setting $X_0 = 1000$ MPa, such that cap would not be attained under the loading conditions used in this work. Figure 13 shows the results in terms of principal stresses and plastic strain intensity for drilling phase and figure 14 presents these results for production phase. Failure occurred in tensile domain at the top of the wellbore during drilling, and the failed region increases during production. Production produces a tensile region at the top of the well, and a high magnitude concentration of tangential stress in X symmetry axis, but no failure is seen in this region.

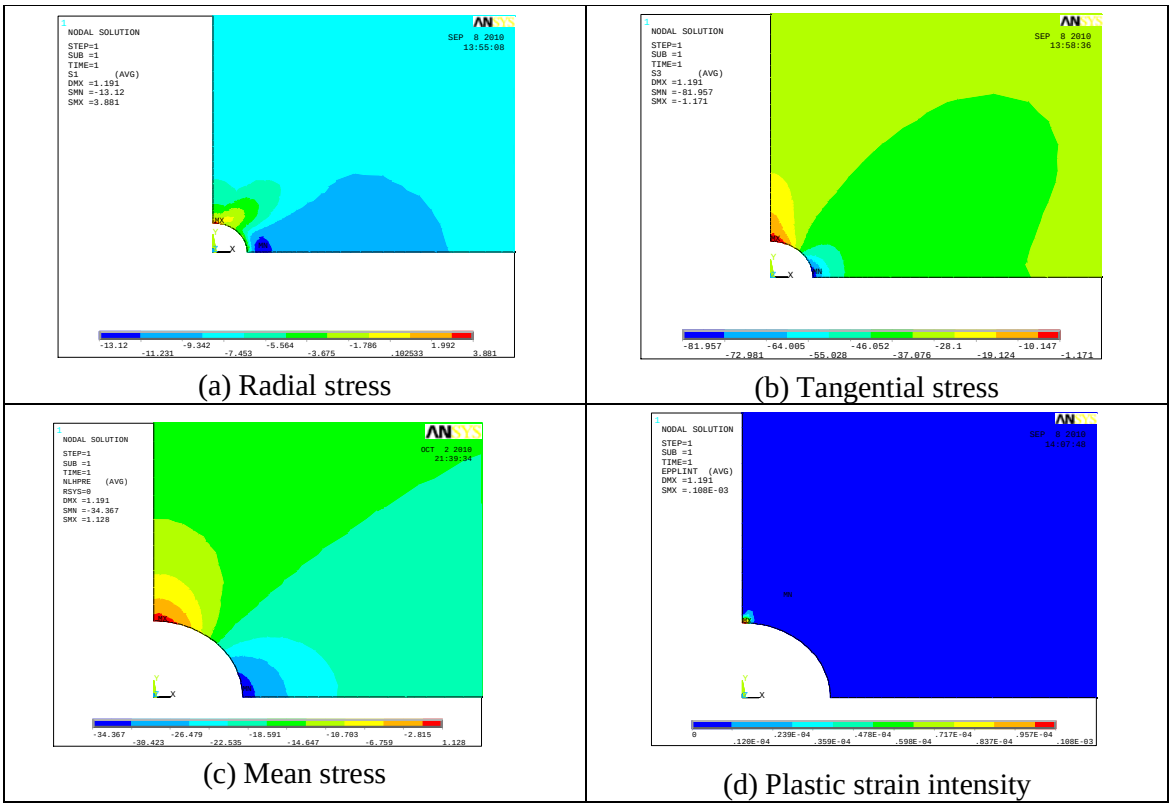

(a) Radial stress (b) Tangential stress

(c) Mean stress (d) Plastic strain intensity

Figure 13: Results for shear failure analysis for drilling phase

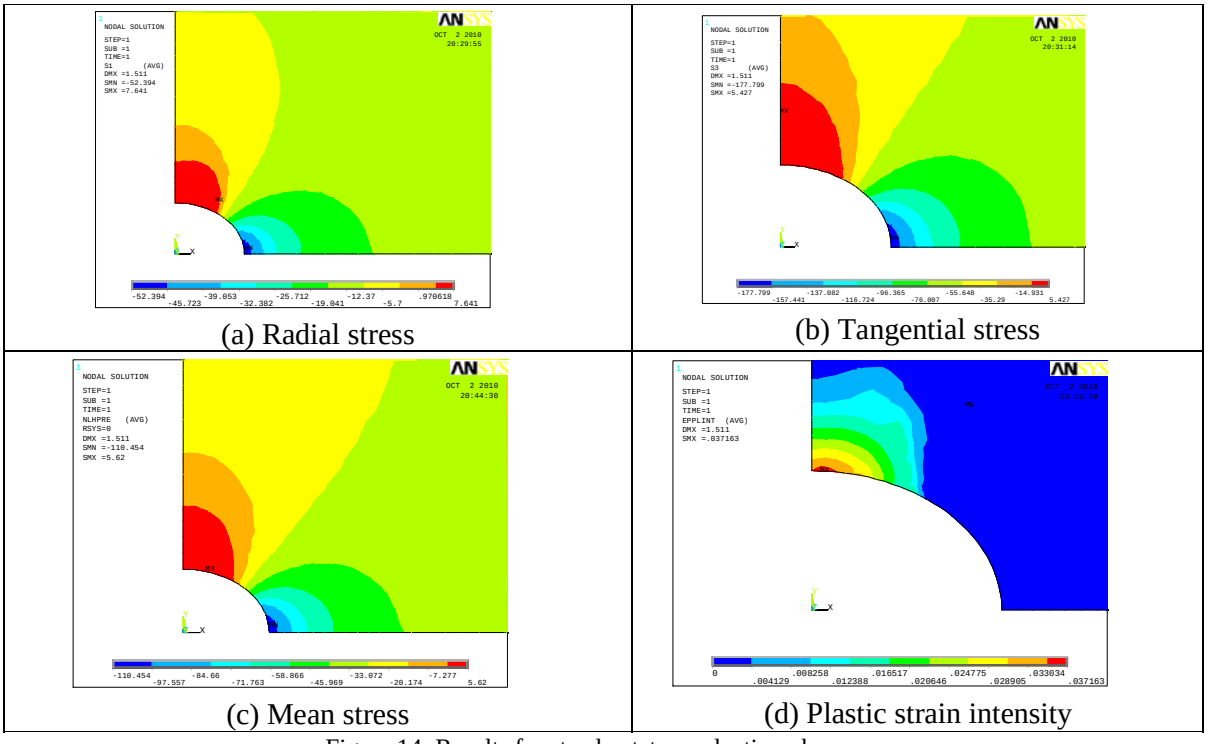

(a) Radial stress (b) Tangential stress

(c) Mean stress (d) Plastic strain intensity

Figure 14: Results for steady-state production phase

6.3 In-situ stress ratio variation

The impact of the in-situ stress ratio was evaluated by changing the horizontal in-situ stress as presented in table 3.

In-situ vertical stress (MPa)	In-situ horizontal stress (MPa)	In-situ stress ratio (MPa)
32	6,4	0,2
32	9	0,3
32	12,8	0,4
32	16	0,5

Table 3 In-situ stress changes.

A summary of the results are presented in the graphic of figure 15.

The contours of principal sresses are presented in figure 16. Mean stress and plastic strain intensity are presented in figure 17.

The higher the horizontal stress, the higher is the confinement around the borehole. Since the cap delimits the confining pressure, it is intuitive to believe that this condition would be more critical to volumetric failure. However, the results show that the critical condition is the higher difference between the in-situ stresses. As the radial stress is prescribed, the effect of the far-field confinement is to relax the tangential stress and reduce plastic strain. It suggests that the failure occurs in the domain described previously as “shear enhanced compaction”.

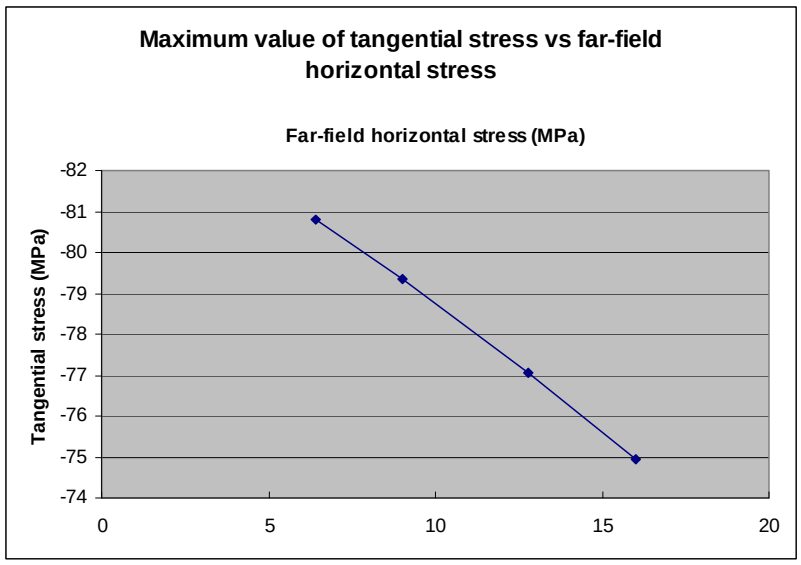

Figura 15: Tangential stress x far-filed horizontal stress

Radial Stress (MPa)	Tangential Stress (MPa)
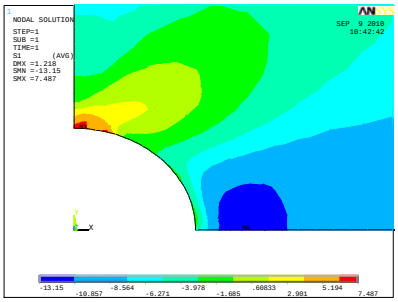	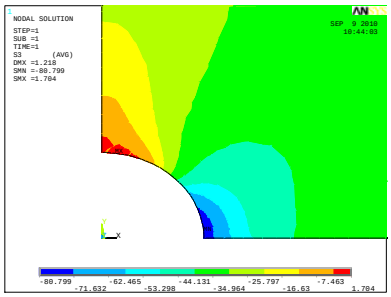
(a) $\sigma_h = 6{,}4$ MPa	(b) $\sigma_h = 6{,}4$ MPa
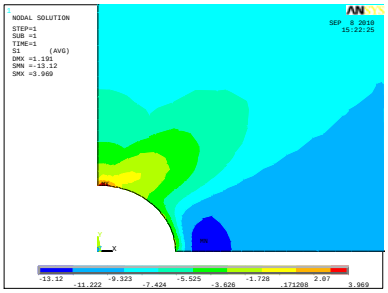	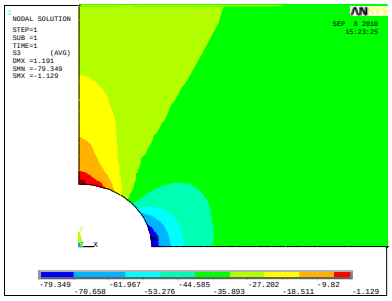
(c) $\sigma_h = 9{,}0$ MPa	(d) $\sigma_h = 9{,}0$ MPa
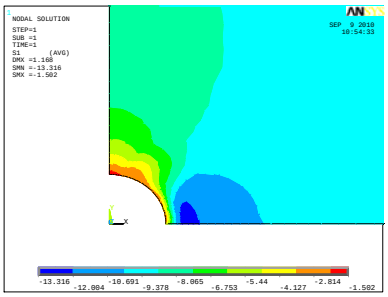	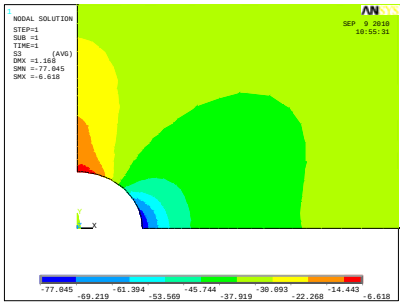
(d) $\sigma_h = 12{,}8$ MPa	(e) $\sigma_h = 12{,}8$ MPa
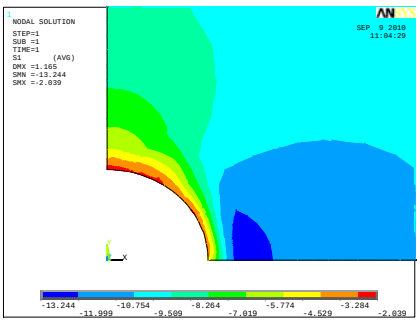	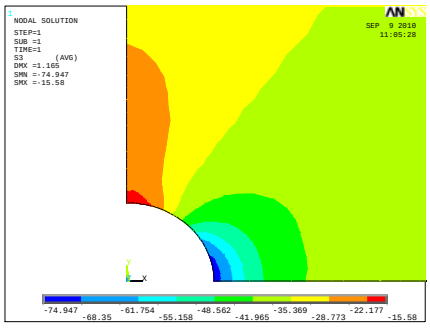
(f) $\sigma_h = 16$ MPa	(g) $\sigma_h = 16$ MPa

Figura 16: Principal stresses for in-situ horizontal stress variation

Mean stress (MPa)	Plastic strain intensity
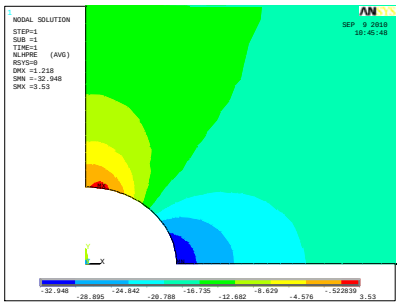	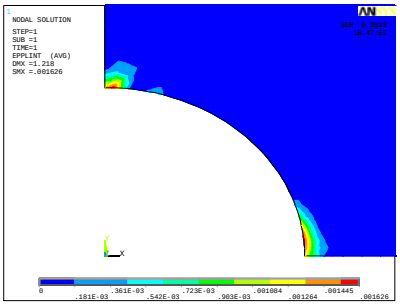
(a) $\sigma_h = 6{,}4$ MPa	(b) $\sigma_h = 6{,}4$ MPa
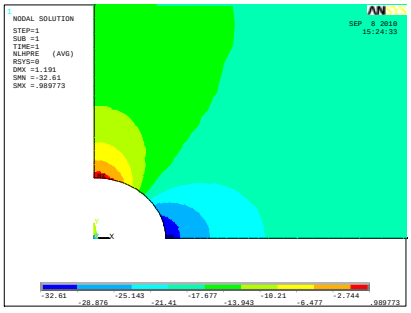	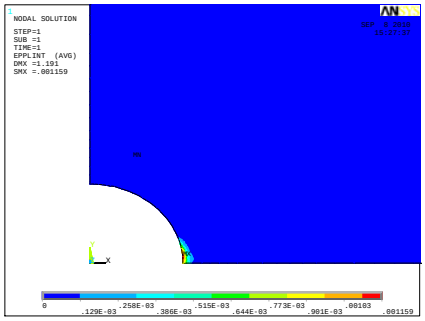
(c) $\sigma_h = 9{,}0$ MPa	(d) $\sigma_h = 9{,}0$ MPa
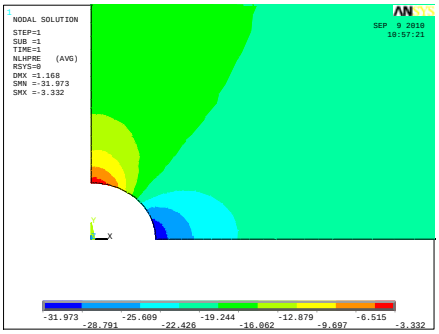	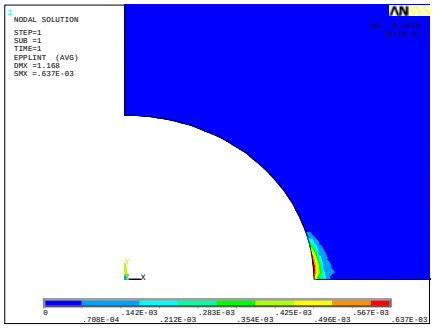
(e) $\sigma_h = 12{,}8$ MPa	(f) $\sigma_h = 12{,}8$ MPa
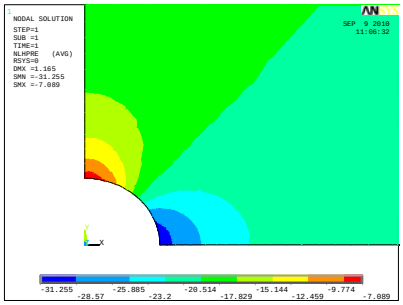	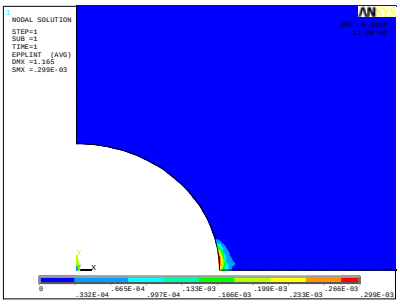
(g) $\sigma_h = 16$ MPa	(h) $\sigma_h = 16$ MPa

Figura 17: Mean stress and plastic strain intensity for in-situ horizontal stress variation

6.4 Effect of borehole pressure

The effect of borehole pressure was evaluated by applying different values of pressure on the cavity: -2, 0, 2 e 4 MPa. Figure 18 shows the graphic major principal stress vs pressure on the boreface. Figures 19 and 20 present the contours of principal stresses, mean stresses and plastic strain intensity.

It can be seen that the reduction on the cavity pressure concentrates tangential stress. This increases the volumetric plastic strain at the borehole wall. As before, the concentration on the tangential stresses is associated to the failure around the well. So, the higher the difference between the principal stresses is the most critical condition, where it seems to occur shear enhanced compaction.

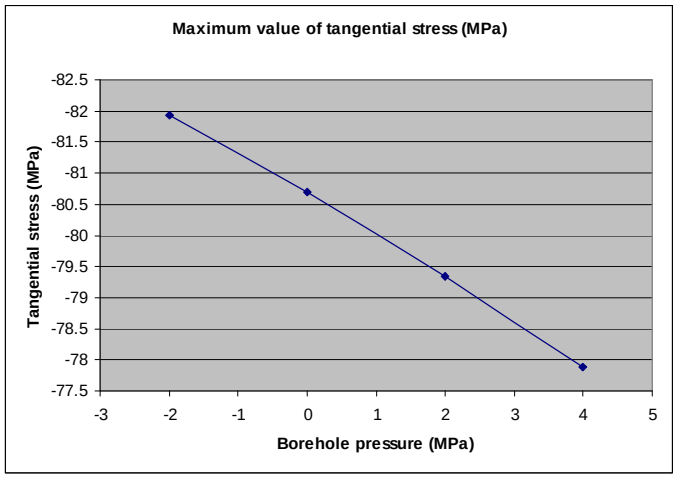

Figure 18: Tangential stress vs cavity pressure

6.5 Production phase

A numerical study on production phase was conducted assuming that the pore pressure on the outer boundaries is equal to the static pressure. At the borehole wall it was assumed a drawdown value of 10 MPa differential pressure.

The changes in pore fluid pressure were evaluated through the poroelastic stresses calculated by analogy with thermoelastic stresses. A pore pressure field was evaluated by thermal steady state analysis. This field was read by the thermostructural analysis and coupled through a compressibility parameter analogous to the thermal expansion coefficient, as described by the equation 20.

In this analysis, the pattern case used in previous models showed instability because both tensile failure and compaction failure. The model did not converge. It was necessary to major the tensile strength by setting the tensile cap parameter R as 2.0. The maximum allowed plastic compressive strain was also enlarged to 0.5.

Figure 21 presents the results for a steady-state analysis considering poroelastic effects, simulating production. It can be seen that production induces radial tensile stresses at the top of the wellbore and compressive stress concentration in the direction normal to the higher in-situ principal stress. The compressive stress concentration at this region associated to tensile failure at the top lead to a large damaged region by volumetric failure.

Radial Stress (MPa)	Tangential Stress (MPa)
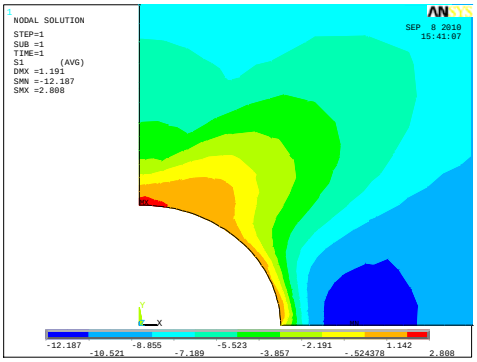	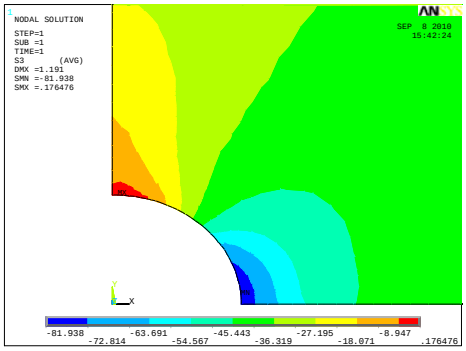
(a) p=-2,0 MPa	(b) p=-2,0 MPa
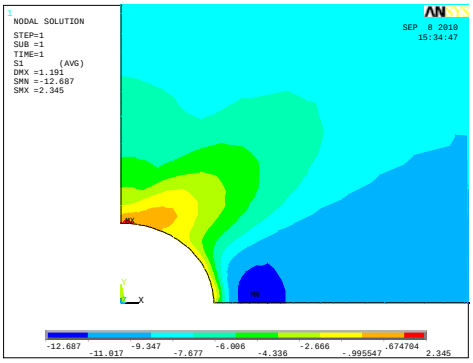	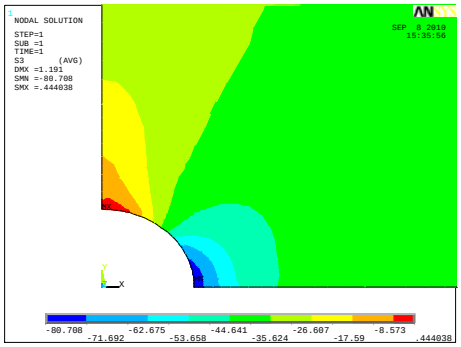
(c) p=0 MPa	(d) p=0 MPa
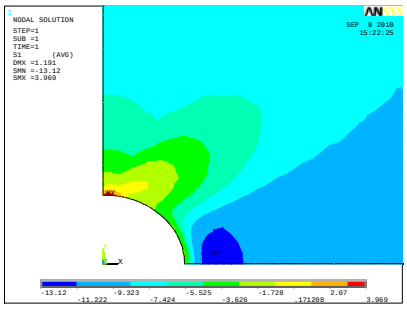	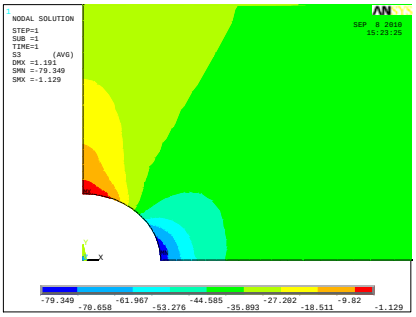
(e) p=2 MPa	(f) p=2MPa
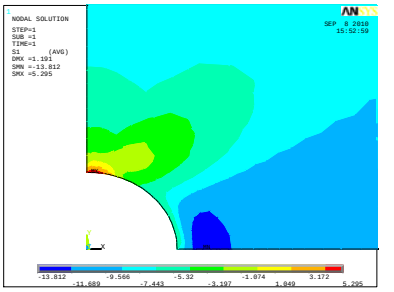	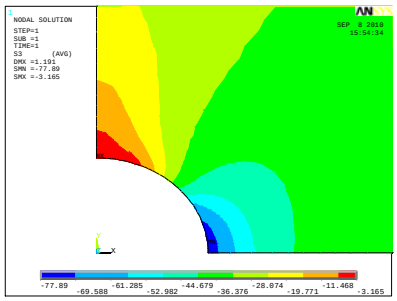
(g) p=4 MPa	(h) p=4 MPa

Figure 19: Principal stresses for pressure changes in the borehole

Mean stress (MPa)	Plastic strain intensity
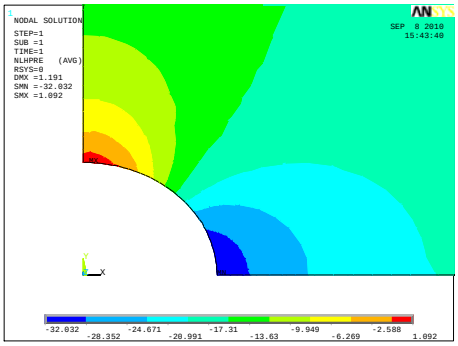	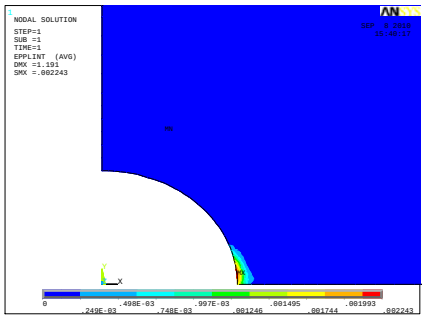
(a) p=-2,0 MPa	(b) p=-2,0 MPa
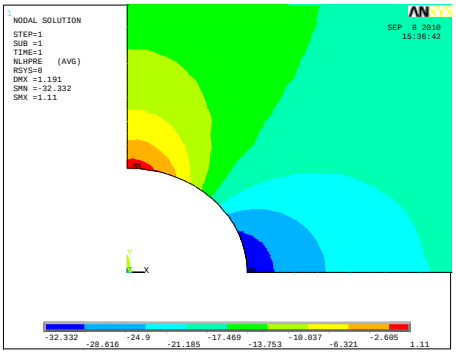	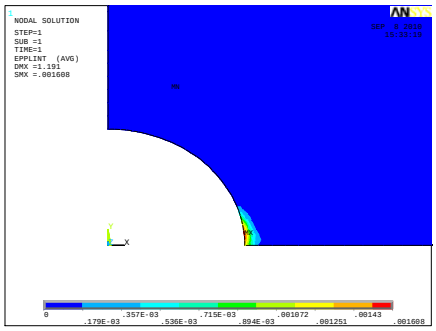
(c) p=0 MPa	(d) p=0 MPa
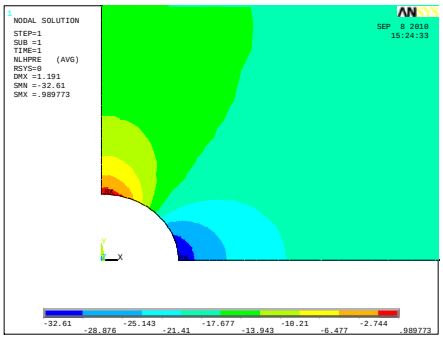	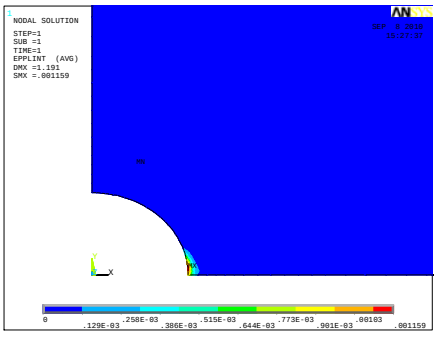
(e) p=2 MPa	(f) p=2MPa
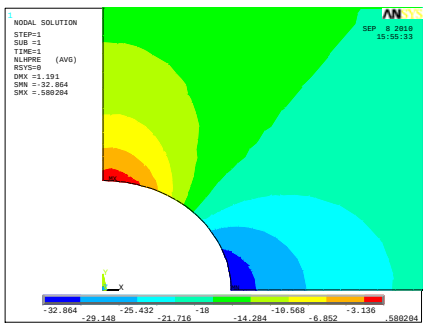	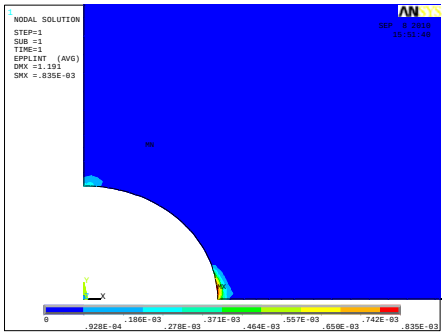
(g) p=4 MPa	(h) p=4 MPa

Figure 20: Mean stress and plastic strain intensity pressure changes in the borehole

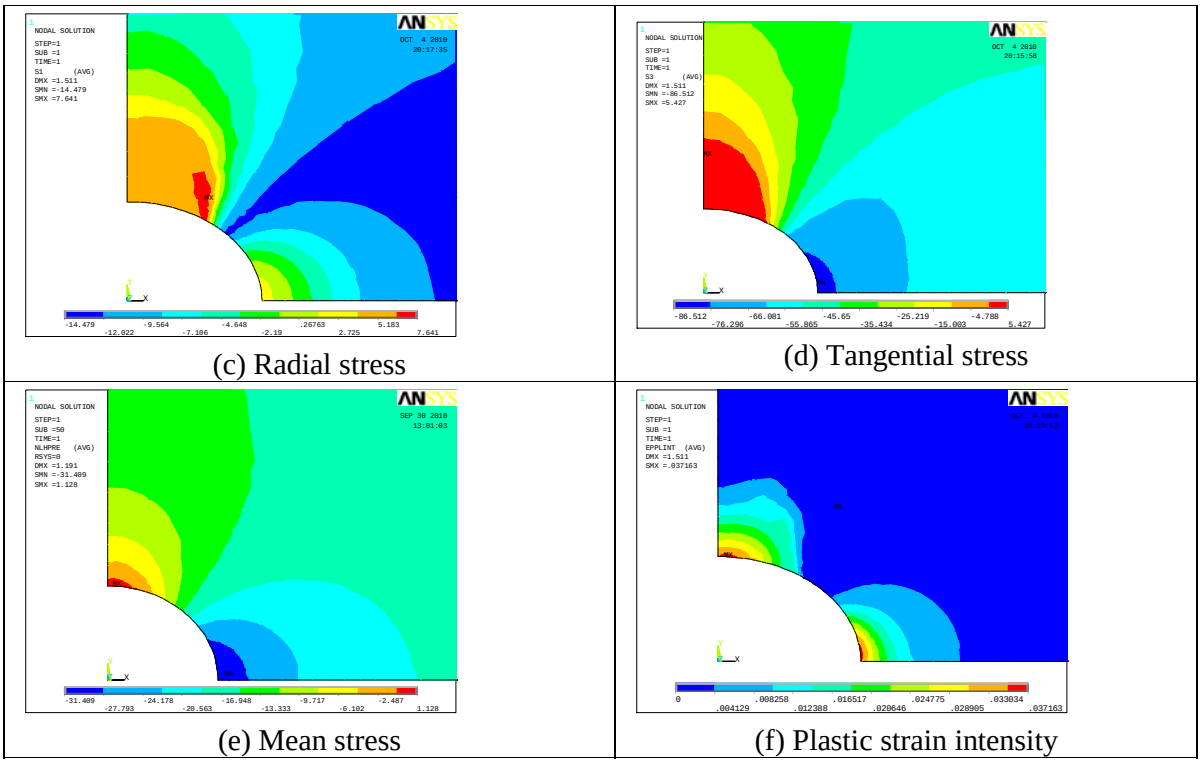

(c) Radial stress (d) Tangential stress

(e) Mean stress (f) Plastic strain intensity

Figure 21: Results for steady-state production phase

7 CONCLUSIONS

The modeling procedure used was able to capture the volumetric compressive behavior of the rock around the borehole. Unlike shear models, as Drucker-Prager or Mohr-Coulomb, which have its parameters well defined and available data for correlation in literature. Cap models present different formulations. To use it, it is necessary to work directly on experimental data, once different formulations lead to different parameters. This is the major drawback of this model.

The analyses presented herein pointed that the tangential stress concentration is critical condition for volumetric failure in horizontal wellbores. During drilling, this tangential stress concentration is higher under high differential in-situ stresses and lower pressure at the boreface. This suggests that the dominant mechanism is shear enhanced compaction. During production, both differential pore-pressure at the bore face and poroelastic effects increase tangential stress, increasing the plastic zone.

Other wellbore configurations and geometries, like directional wellbores or anisotropic stress states will be evaluated to a better understanding or volumetric failure. The role of rock anisotropy should be also investigated.

Elastic-plastic cap plasticity models are able to define a damaged zone. The size of plastic zone that induce borehole instability is a matter of research. In the field, this mechanism is not completely understood. It is known that plastic compaction disaggregates the material, causing debonding and grain breakage. Whether this material will be carried by fluid flow or it will produce a compacted region that acts as a barrier to flux should be investigated by more refined coupled models. Localization models, multiscale models or FEM-DEM coupling would be helpful in understanding the role of compaction in wellbore instability.

AKNOWLEDGEMENTS

The authors are thankful to Fundação de Amparo à Pesquisa do Rio de Janeiro and Agência Nacional do Petróleo for their partial support to this research.

REFERENCES

Baud, P., Coelho, L.C., Alves, J.L.D., Guevara Jr., N.O., Wong, T-F, Inelastic deformation and strain localization in carbonate rocks: experimental data and constitutive modeling. *Proceedings of XXIX Iberian Latin American Congress on Computational Methods in Engineering*, Maceió, 2008.

Baud, P., Klein, E., Wong, T-F., Compaction localization in porous sandstones: spatial evolution of damage and acoustic emission activity. *Journal of Structural Geology*, 26: 603-624, 2004.

Baud, P., Vajdova, V., Wong, T-F., Shear-enhanced compaction and strain localization: inelastic deformation and constitutive modeling of four porous sandstones. *Journal of Geophysical Research*, 111: B12401, doi: 10.1029/2005JB004101, 2006.

Bradley, W.B., Failure of inclined boreholes. *Journal of Energy Resourses Technology*, 101:232-239, 1979.

Coelho, L.C., Soares, A., Ebecken, N., Alves, J.L., and Landau, L., The impact of constitutive modeling of porous rocks on 2-D wellbore stability analysis, *Journal of Petroleum. Science and Engineering*, 46: 81-100, 2005.

Detournay, E. and Cheng, A.H-D, Fundamentals of poroelasticity, Chapter 5 in *Comprehensive Rock Engineering: Principles, Practice and Projects*, *Vol. II, Analysis and Design Method*: 113-171, ed. C. Fairhurst, Pergamon Press, 1993.

Ewy, R.T., Wellbore Stability Predictions Usina a Modified Lade Criterion. *SPE Eurorok 98,* Trondhelm, Nonway, 08-10 July 1998.

Fjaer, E., Holt, R.M., Horsrud, P., Raaen, A.M., Risnes, R., *Petroleum related rock mechanics*, 2nd Edition. Elsevier, 2008.

Haimson, B., Micromechanisms of borehole instability leading to breakouts in rocks. *International Journal of Rock Mechanics and Mining Sciences,* 44: 157-173, 2007.

Haimson, B.C., Song, I, Borehole breakout in Berea sandstone: two porosity-dependent distinct mechanisms of formation. *SPE/ISRM Eurorock 98*. Trondheim, Norway, 8-10 julho, 1998.

Morita, N., Well Orientation Effect on Borehole Stability. *SPE Annual Technical Conference and Exhibition*, 26-29 September 2004, Houston, Texas, SPE paper 89896-MS, 2004.

Papanastasiou P. and Vardoulakis I. (1989). Bifurcation analysis of deep boreholes: II. Scale effect. *Int. J. Num. Anal. Meth. Geomechanics*, 13, 183-198.

Vajdova, V., P. Baud, and T.-f. Wong, Compaction, dilatancy and failure in porous carbonate rocks. *Journal of. Geophysical Research*, 109: doi:10.1029/2003JB002508, 2004.

Vardoulakis I. and Papanastasiou P., Bifurcation analysis of deep boreholes: I. Surface Instabilities. *Int. J. Num. Anal. Meth. in Geomechanics*, 12: 379-399, 1988.

Wang Y.1; Dusseault M.B. A coupled conductive-convective thermo-poroelastic solution and implications for wellbore stability. *Journal of Petroleum Science and Engineering*, Volume 38: 187-198, 2003.

Yu, M, Chevernet, M.E., Sharma, M.M., Chemical–mechanical wellbore instability model for shales : accounting for solution diffusion. *Journal of Petroleum Science and Engineering*, 38:131-143, 2003.

Zang, L., Zhu, H., Three-Dimensional Hoek-Brown Strength Criterion for Rocks. *Journal of Geothecnical and Geoenvironment Engineering*, 113: 1128-1135, 2007.

Zervos,A. Vardoulakis, I., Papanastasiou, P., Influence of Nonassociativity on Localization and Failure in Geomechanics Based on Gradient Elastoplasticity. *International Journal of Geomechanics*, 7: 63-74, 2007.